Curved Waveguide Array Diode Lasers for High-Brightness Applications

V. C. Elarde, K. E. Tobin, R. K. Price, V. B. Verma, *Student Member, IEEE*, and J. J. Coleman, *Fellow, IEEE*

***Abstract*—We have developed a novel structure for achieving high-brightness output from a semiconductor laser array using coherent spatial beam combination. The structure consists of an array of curved ridge waveguides with in-phase, coherent output. Interference of the multiple outputs leads to a narrow, bright, on-axis, far-field beam shape. Experimental results demonstrate a diffraction limited output beam width, ideal for high-brightness applications.**

***Index Terms*—Coherent array, high-brightness, semiconductor laser, spatial beam combination.**

I. Introduction

SEMICONDUCTOR laser arrays are advantageous over single element systems for high-power applications because the total power output of the device can be divided among many individual elements. However, the output of such an array typically has a very poor beam quality. A suitable mechanism for combining the outputs of the many elements of a laser array must therefore be used in order to achieve an improvement in brightness. In this letter, we present a waveguide structure containing multiple array elements with coherent, in-phase outputs such that interference effects lead to a nearly diffraction-limited combined output.

Many methods of providing coherent coupling among elements of the array, such as that of Leger, *et al.* [1], use external lenses and mirrors to provide feedback between adjacent elements. While this technique has been demonstrated to work, the fabrication is complicated by the need for several discrete components and precision alignment between these components.

Combining individual elements of semiconductor laser diode arrays has been attempted using several different techniques in recent years and is well summarized by Fan [2]. One very recent report by Causa, *et al.* [3] describes the use of an array of parabolic bow-tie lasers. Under certain operating conditions, these devices achieve in-phase coupling. Under other conditions, the devices demonstrate out-of-phase coupling, indicating a certain level of instability in the coupling characteristics of these devices.

Finally, Y-junction coupled semiconductor laser arrays have been used to achieve in-phase coupled high-brightness arrays [4], [5]. In this method, an array of narrow stripe semiconductor lasers is coupled together by a series of Y-junctions. This structure can be tuned to select the in-phase mode by ensuring that mode has the minimum loss.

Manuscript received August 10, 2007; revised March 4, 2008. This work was supported in part by Nuvonyx, Inc., under Air Force Subcontract 2007-00253.

The authors are with the Department of Electrical and Computer Engineering, University of Illinois, Urbana, IL 61822 USA (e-mail: vcelarde@uiuc.edu).

Digital Object Identifier 10.1109/LPT.2008.924299

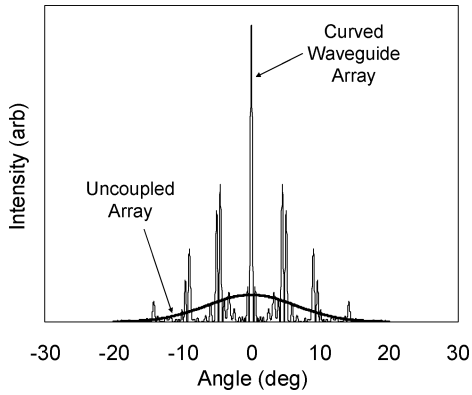

Fig. 1. Calculated far-field output pattern for the curved waveguide array device and an otherwise identical array with uncoupled elements. Constructive interference of the output beams results in a high-brightness central lobe.

II. Design Concept

The goal of this work is to achieve high spatial and spectral brightness output from a semiconductor lasers array via spatial beam combination from an array of in-phase coherently coupled emitters. This goal is achieved through the use of an array of curved waveguides. The waveguides consist of three regions: the coupling region, the phase shift region, and the output region. In the coupling region, the waveguides are very close together such that the guided modes will couple evanescently. It is expected that the phase of the optical field in adjacent waveguides will be 180° out of phase, since this supermode will experience the minimum amount of loss. In the phase shift region, the waveguides curve away from each other. This region transforms the lateral optical mode from a strongly coupled supermode in the coupling region to an array of independent Gaussian-like modes at the output facet.

The phase shift region also adjusts the relative phase of the optical field in the waveguide array such that the individual Gaussian modes at the output of the device are in phase. The curvature function which defines the shape of the waveguide is constructed such that the differential path length of adjacent waveguides is an odd number of half-wavelengths of light scaled by the effective refractive index of the waveguide. Propagation of light through the phase shift region, therefore, results in a relative phase shift of every other waveguide by a factor of π, yielding an array of separate, Gaussian-like, in-phase emitters at the output facet of the waveguide array. Constructive interference of the outputs of this array results in a far-field pattern containing a central lobe with higher brightness than could be achieved with an uncoupled array.

Fig. 1 is a plot of the calculated far-field output from this structure as well as the output from an uncoupled, but otherwise identical, array. The central lobe of the far-field pattern of the

curved waveguide array is 12 times brighter than the Gaussian far-field pattern of an uncoupled array for the case of normalized total output power, despite the power lost to the side lobes, due to its much narrow angular distribution.

This structure is expected to achieve high *spectral* brightness as well via selection of the particular resonance frequency where the Fabry–Perot spectra of the individual waveguides are aligned.

The geometry of the curved waveguides is defined mathematically by the following Lorentzian function:

$$y_n(x_n) = \int_{x=0}^{x_n} \left[\frac{\frac{1}{2\pi}(w_0 + |nw|)}{(x - x_0 - |np|)^2 + \left(\frac{w_0 + |nw|}{2}\right)^2} M(n)\, dx \right] + ns.$$

In this equation, $y_n(x_n)$ is the lateral position of each waveguide, given as a function of x_n, the longitudinal position of each waveguide. n is the waveguide number. All of the devices tested in this experiment contained 11 waveguides, therefore n varied from -5 to $+5$. p_0 is the longitudinal position of maximum curvature corresponding to the peak of the Lorentzian curvature function. P is a parameter which characterizes the longitudinal shift of the peaks of the Lorentzian functions for neighboring waveguides. For this experiment, p_0 was set to 1500 μm (from the back facet) in order to allow for strong coupling between the waveguides by keeping them close together over roughly two-thirds of the cavity length. P was set to 20 μm to ensure the waveguides were decoupled for the majority of the phase shift region. w_0 and w characterize, respectively, the full-width of the Lorentzian curvature functions and the variation in full-width between neighboring waveguides. In this experiment, w_0 was set to 30 μm and w was set to 10 μm. s is the center-to-center spacing between adjacent waveguides at the back facet of the device and was varied from 4 to 8 μm. $M(n)$ is the magnitude of the Lorentzian curvature function. This parameter was determined for each waveguide such that the total length of each waveguide was an odd number, b, of half wavelengths different from its neighbors through numerical solution of the following:

$$L_n = \int_{x=0}^{L_c} \sqrt{dx^2 + \left(\frac{\frac{1}{2\pi}(w_0 + |nw|)}{(x - x_0 - |np|)^2 + \left(\frac{w_0 + |nw|}{2}\right)^2} M(n)\, dx \right)^2} = L_c + \frac{b\lambda\,|n|}{2}.$$

The differential path length between neighboring waveguides was varied from 1 to 11 half-wavelengths in this experiment ($b = 1$ to 11). L_c in the above equation is the physical distance between the device facets. Due to the curvature of the waveguide, the optical path length is increased to L_n. λ is the wavelength of light in the waveguide, and n, as previously, is the waveguide number. The width of each waveguide was 4 μm.

In order to allow for error in the cleaving of individual devices, 100 μm of the waveguides are forced to be straight at either end of the device. As long as the cleaves which form the device facets fall within the straight segments, the phase relationship between the emitters will not be affected, aside from a minute shift in the resonance frequency at which all the Fabry–Perot resonances of the various waveguides are aligned.

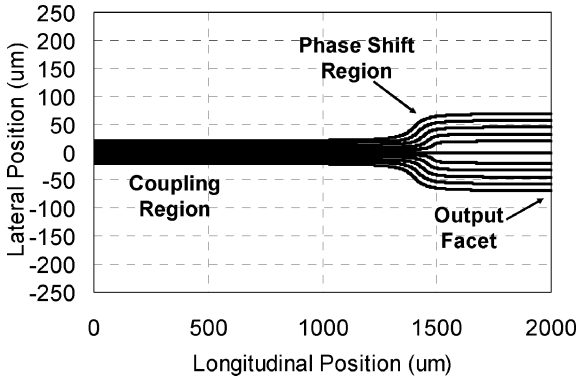

Fig. 2. Plot of the ridge waveguide geometry for the best performing design containing 11 waveguides with a seven half-wavelength differential length between waveguides. The waveguides merge in the coupling region into a 44-μm -wide broad area ridge.

In this experiment, several different waveguide geometry designs were tested. Waveguide differential lengths of 1, 3, 5, 7, 9, and 11 half-wavelengths and center-to-center spacings at the back facet of 4, 5, 6, 7, and 8 μm were combined in a design matrix to form 30 unique device types. Note that for the 4-μm center-to-center spacing designs, the waveguides merge into a single 44-μm waveguide. Far-field measurements were made over a range of injection currents from threshold to 500 mA on devices based on each of these designs. The devices which presented a far-field pattern indicative of coherent phase matching were determined to have the optimum waveguide geometry design. The optimum design had a waveguide differential length of 7 half-wavelengths and a center-to-center spacing at the back facet of 4 μm. The experimental results for the design demonstrating the desired waveguide coupling are presented as follows. Fig. 2 contains a plot of the waveguide geometry for this design.

III. Results

A variety of specific waveguide geometries were tested to determine which provided the strongest in-phase coherent coupling. The best performing structure had 11 4-μm-wide waveguides at the front end of the device which merged into a broad 44-μm-wide waveguide at the back end. The difference in length of adjacent waveguides in this design was seven half-wavelengths. A plot of the waveguide geometry for this structure is presented in Fig. 2.

The device was tested under pulsed current injection with 2-μs pulses and a 0.3% duty cycle. The threshold current of 212 mA corresponds to 19.3 mA/emitter. The light-versus-current curve was found to be kink-free over the range of currents tested, indicating stable lateral mode operation in this range. The light versus current and voltage versus current from this device is presented in Fig. 3. The spectral output of these devices was found to be predominantly single mode. The spectrum is presented in Fig. 4. Side lobes were observed in the spectrum which

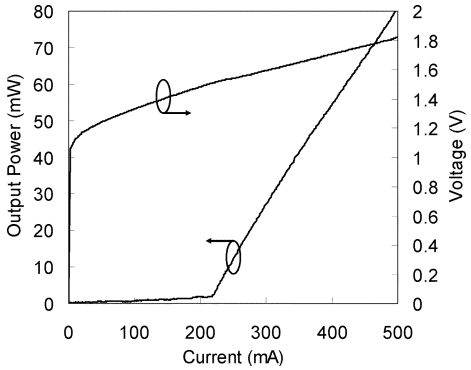

Fig. 3. Light versus current and voltage versus current for the 11–element curved waveguide array. The threshold current of 212 mA corresponds to 19.3 mA/emitter.

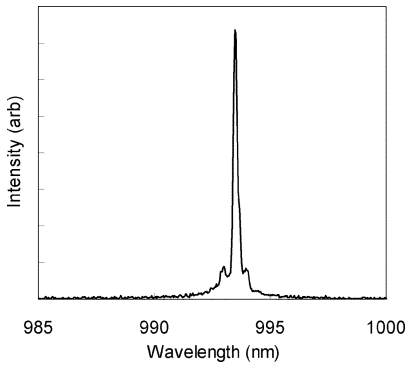

Fig. 4. Spectral output of a curved waveguide array device. The emission spectrum is predominantly single mode. Side lobes were observed and are likely the result of misalignment between the design wavelength of 980 nm and the peak gain. The measurement was taken with a spectral resolution of 1 Å at 300 mA, approximately 1.5 × threshold.

are likely due to a misalignment between the design wavelength of 980 nm and the peak of the gain wavelength at $\sim$ 994 nm.

The near-field image taken from this device contains 11 distinct Gaussian-like modes, corresponding to output from the 11 individual waveguides of the array. The near-field image is presented in the inset of Fig. 5. The far-field output pattern from this device contains multiple peaks, indicating interference of the output from the individual waveguides. The single, on-axis, central lobe indicates that the fields in the individual waveguides are in-phase. The measured far-field data is presented in Fig. 5.

The $1/e$ beam width of the central lobe was 1.6°, which is approximately the diffraction limit for a laser array of this geometry. The Strehl ratio was calculated for this device by comparing the peak of the experimentally measured, normalized far-field at 500 mA (Fig. 5) to that of the calculated far-field (Fig. 1) and was found to have a value of 0.23. While this value represents less than ideal performance, the on axis-intensity is still a factor of 2.5 greater than could be theoretically achieved from an ideal, conventional array without the curved waveguide structure.

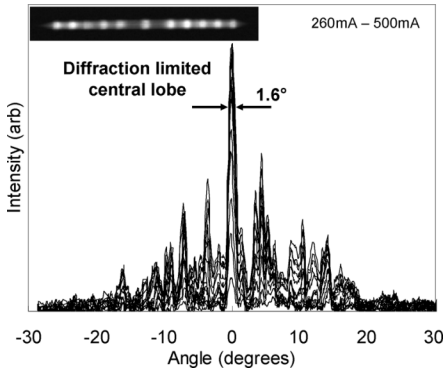

Fig. 5. Far-field profile from the curved waveguide array device containing 11 elements. The narrow, on-axis central output lobe suggests strong in-phase coherence of the emission from the individual elements. Inset: Near-field image from the same device, taken at 300 mA, showing 11 distinct output modes. The near-field pattern remains constant up to the maximum current tested (500 mA).

IV. Conclusion

In this letter, we have developed a novel curved waveguide array structure designed to achieve constructive interference of the array elements in the far field. The structure is designed to produce an array of coherent, in-phase, Gaussian-like output beams at the facet which spatially combine to form a single, on-axis, diffraction limited beam pattern in the far field. The prototype device presented here has achieved a Strehl ratio 2.5 times greater than what could theoretically be achieved by a conventional semiconductor laser array. The device has thus far been presented at low operating power to demonstrate the coherent, spatial combination of the output beams of the array. Future work will include cw operation of the device at high power which is expected to be achievable with proper heat sinking and facet coating.

Acknowledgment

The authors would like to thank D. Roh with Nuvonyx, Inc., for contributions to this work.

References

[1] J. R. Leger, M. L. Scott, and W. B. Veldkamp, "Coherent addition of AlGaAs lasers using microlenses and diffractive coupling," *Appl. Phys. Lett.*, vol. 52, pp. 1771–1773, 1988.

[2] T. Y. Fan, "Laser beam combining for high-power, high-radiance sources," *IEEE J. Sel. Topics Quantum Electron.*, vol. 11, no. 4, pp. 567–577, Apr. 2005.

[3] F. Causa and D. Masanotti, "Observation and analysis of phase-locking in parabolic bow-tie laser arrays," *IEEE J. Quantum Electron.*, vol. 42, no. 10, pp. 1016–1022, Oct. 2006.

[4] W. Streifer, D. Welch, P. Cross, and D. Scifres, "Y-Junction semiconductor laser arrays: Part I–Theory," *IEEE J. Quantum Electron.*, vol. 23, no. 6, pp. 744–751, Jun. 1987.

[5] D. Welch, W. Streifer, P. Cross, and D. Scifres, "Y-Junction semiconductor laser arrays: Part II–Experiments," *IEEE J. Quantum Electron.*, vol. 23, no. 6, pp. 752–756, Jun. 1987.